IEEE Access
Multidisciplinary ⋮ Rapid Review ⋮ Open Access Journal

Received January 13, 2022, accepted February 5, 2022, date of publication February 9, 2022, date of current version February 25, 2022.

Digital Object Identifier 10.1109/ACCESS.2022.3150278

Sub-6 GHz Highly Isolated Wideband MIMO Antenna Arrays

AMANY A. MEGAHED[1], MOHAMED ABDELAZIM[2], EHAB H. ABDELHAY[2], AND HEBA Y. M. SOLIMAN[3], (Senior Member, IEEE)

[1]Higher Institute of Engineering and Technology, New Damietta 41525, Egypt
[2]Electronic and Communication Department, Mansoura University, Mansoura 35516, Egypt
[3]Electronic and Communication Department, Port Said University, Port Fuad 42526, Egypt

Corresponding author: Heba Y. M. Soliman (hebayms@eng.psu.edu.eg)

ABSTRACT This study proposes a compact four-port multiple-input multiple-output (MIMO) antenna system to operate within a frequency range of 3.2–5.75 GHz to serve in 5G new radio (NR) sub-6 GHz n77/n78/n79 and 5 GHz WLAN with good impedance matching. To increase the isolation between the MIMO antenna elements with low complexity and cost, the antenna elements are orthogonally oriented to each other with distance spacing of $0.3\lambda_o$ between elements, including electromagnetic bandgap (EBG) structure, defected ground structure (DGS), capacitive elements (CE), and neutralization line (NL). The simulation results show that the measured mutual coupling between the array elements is improved from −20 to −45 dB. The envelope correlation coefficient is enhanced. In addition, the diversity gain, mean effective gain, and total active reflection coefficient are improved simultaneously. The suggested structure has been designed on CST Microwave Studio 2019. The antennas' overall dimensions for all methods are the same as they approach 46 mm × 46 mm × 1.6 mm. The measured gain of the proposed designs ranges from 6 to 9 dBi, and the radiation efficiency approaches 90%. The antennas are fabricated and tested, where better experimental results are noticed compared to the simulation results. Our antennas are designed over FR-4 substrate with a noticeable cost reduction. Each antenna element has a dimension of 15 mm × 23 mm × 1.6 mm. An ''EL'' slot into the radiating element and two identical stubs coupled to the partial ground are used to improve the impedance matching and radiation characteristics across the bands of interest. The isolation decreases by 22 dB using the EBG method, reaching the value of −65 dB. Meanwhile, the isolation decreases by 19 dB using the DGS method, reaching −60 dB. Due to gaps between adjacent unit cells and the capacitance generated from the dielectric gap between the top metallic patch and ground plane, the EBG method gives the best results. However, in the CE method, capacitances resulting from the four transmission lines in the bottom side of the antennas (parasitic elements) decrease the isolation by 15 dB, reaching −40 dB. NL method makes the isolation to reach the value of −55 dB. Accordingly, the proposed antenna arrays support 5G NR sub-6 GHz n77/n78/n79 and 5 GHz WLAN, where n77 (3.3–4.2 GHz), n78 (3.3–3.80 GHz), and n79 (4.4–5.0 GHz) require a wideband coverage that extends from 3.3 GHz to at least 5.0 GHz.

INDEX TERMS 5G, multiple-input multiple-output antennas, ECC, DG, MEG, TARC, DGS, and NL.

I. INTRODUCTION

Small size wideband microstrip patch antenna with partial ground design is a major challenge. Multiple-input multiple-output (MIMO) antenna technology is one of the most important technologies in the 5G wireless communication system. This technology develops spectrum Small size wideband microstrip patch antenna with partial ground design is a major challenge. Multiple-input multiple-output (MIMO) antenna technology is one of the most important technologies in the 5G wireless communication system. This technology develops spectrum efficiency, energy, and cost efficiency. MIMO has been widely used in different systems to significantly develop channel capacity. In addition, MIMO systems are used in several applications [1]–[3]. Compact array antennas are often used due to space limitations and aesthetic reasons. In [4], a MIMO antenna array with narrow bandwidth and gain up to 6 dBi has been presented. Wu *et al.* [5] presented

The associate editor coordinating the review of this manuscript and approving it for publication was Jiankang Zhang.

a four-port MIMO antenna array with a band notch that uses electromagnetic bandgap (EBG) to reduce mutual coupling. The band notch is centered at 4.6 GHz covering the band from 4 to 5.2 GHz with isolation of 17.5 dB between ports with dimensions of 60 mm × 60 mm × 1.6 mm using FR-4 substrate. The relative permittivity, efficiency, and gain are 4.4, 90%, and 8 dBi, respectively. Several attempts have been made to improve the bandwidth by cutting the resonant slot inside the patch [6]. The main problem in designing a MIMO antenna array is mutual coupling. Numerous studies used various methods to decrease the effects of this problem. In [7], a two-port MIMO antenna array using defected ground structure (DGS) to obtain high isolation between ports with dimensions of 45 mm × 45 mm × 1.6 mm has been presented. The isolation is less than 14 dB. The gain and peak efficiency of the array are 4 dBi and 91%, respectively. The bandwidth ranges from 2.2 to 6.28 GHz. The antenna is designed on an FR-4 substrate. Luo *et al.* [8] presented an H-shaped antenna placed in a square loop with FR-4 substrate while covering the band from 5.2 to 5.8 GHz with isolation of 14 dB between ports. The gain of the proposed antenna is approximately 5 dBi, and the efficiency approaches 80%. The antenna dimensions are 42 mm × 42 mm × 0.8 mm with a noticeable size reduction compared to [5], [7]. In [9], a four-port MIMO antenna array with a size of 40 mm × 30 mm × 1.6 mm with a noticeable size reduction compared to [5], [7], [8] has been introduced. The bandwidth ranges from 3.2 to 5.7 GHz, and it is fabricated on FR-4 substrate. The isolation of the antenna array using DGS is less than −10 dB, especially S_{31}, and this result is not sufficiently good. The gain of the proposed antenna is about 3.5 dBi, and the efficiency approaches 82%. Meanwhile, Yang and Zhou [10] presented a circular patch and L-shaped as an isolating element decoupling structure with a compact size of 30 mm × 30 mm × 0.8 mm with a noticeable size reduction compared to [5], [7]–[9] with FR-4 substrate. The gain of the proposed antenna is approximately 4.35 dBi, efficiency approaches 75%, isolation is up to 15.4 dB, and bandwidth ranges from 4.58 to 6.12 GHz. In [11], a compact dual-band MIMO antenna array for 5G smartphone with FR-4 substrate with a size of 124 mm × 74 mm × 4 mm (eight-element) with a noticeable increase in size compared to [5], [7], [8]–[10] that covers the band from 3.3 to 3.6 GHz and 2.4 to 2.7 GHz with isolation of 15.1 dB has been presented. The efficiency ranges from 60% to 80%. A decoupling antenna array with an X-shaped strip and a large size of 152 mm × 50 mm × 1 mm with gain reaches 13.6 dBi with a noticeable increase compared to [5], [7], [8]–[11] has been presented [12]. The isolation is not good enough, as S_{21} is −6.15 dB; S_{31} is −9.00 dB; and S_{14} and S_{15} are reduced by 10.41 and 15.11 dB, respectively. The array is complex in design as it consists of two Rogers/duroid 5880 substrates, with a relative permittivity of 2.2 and a loss tangent of 0.001. It is separated by an air gap with a noticeable increase in cost. In [13], a Quasi-Yagi hybrid wideband decoupling structure, consisting of multiple slots, a rake-type locker, and an I-shaped isolator with a size of 45 mm × 59.6 mm × 0.5 mm using FR-4 substrate has been introduced. The bandwidth ranges from 4.7 to 10.6 GHz, and the gain is above 8 dBi with isolation of −12.2 dB. Sourav Roy *et al.* [14] proposed a meta-inspired decoupling method to reduce the isolation with a bandwidth of 1.34 to 3.92 GHz and 4.34 to 6.34 GHz. The gain ranges from 3 to 5 dBi with dimensions of 100 mm × 60 mm × 1 mm and isolation of −10 dB. It is designed and fabricated on a jean's substrate, which has a dielectric permittivity of 1.6 and loss tangent of 0.02. Meanwhile, in [15], a four-port MIMO dipole array using neutralization lines (NL) to reduce mutual coupling between ports has been introduced. The design is printed on the FR-4 substrate of size 45 mm × 60 mm × 1.6 mm. It provides isolation below −20.55 dB with a bandwidth of 2.09 to 2.68 GHz and 4.73 to 6.33 GHz. In [16], a two-port MIMO array using NL has been provided to reduce mutual coupling. The design is printed on a 35 mm × 33 mm × 0.8 mm FR-4 substrate. The gain and efficiency are 5 dBi and 80%, respectively, and the bandwidth ranges from 3.1 to 5 GHz with more than 22 dB isolation. In [17], a 4 × 4 antenna array using a meta-surface superstrate has been designed. The design is printed on a 110 mm × 110 mm × 1.52 mm substrate. The array is printed on a substrate of RO4350B. The gain and efficiency are 5 dBi and 77%, respectively, and the antenna operates at 5.8 GHz. In [18], a 2 × 2 antenna array using floating parasitic elements to provide isolation with −15 dB has been designed. The design is printed on a 40.5 mm × 26 mm × 1.524 mm substrate. The array is printed and fabricated on a Rogers TMM4 substrate with a dielectric constant of 4.5. The gain and efficiency are 5.75 dBi and 85%, respectively, and the antenna covers the band from 3 to 8.5 GHz. In [19], the meta-surface concept has been presented to suppress the mutual coupling between the radiation parts using a 2 × 2 antenna array with an edge-to-edge distance of $0.16\lambda_o$ between the radiation components. The array covers the band from 8.2 to 12 GHz. The array is constructed of four circular patches implemented on the FR-4 substrate. It exhibits an average efficiency and gain of 76% and 8.5 dBi, respectively. Compared to the proposed design, higher efficiency and gain are achieved by our proposed design. Xu *et al.* [20] used metamaterial loading techniques and DGS in array design to reduce mutual coupling. In [21], eight-port UWB MIMO antenna with a parasitic decoupling structure at antenna rear-sides has been designed to reduce mutual coupling. Sharma *et al.* [22], uses DGS in designing the structure of the antenna to give high isolation, low correlation coefficient, and suppressed cross-polarization with high gain.

In this study, we employ the design of a single element from [9] and improve some changes in dimensions to obtain better results and performance improvement. Next, we design an orthogonal four-port MIMO antenna array to reduce mutual coupling using different methods. We introduce four methods of isolating structures between elements and compare these methods. The proposed antenna array supports 5G new radio (NR) sub-6 GHz n77/n78/n79 and 5 GHz

WLAN, where n77 (3.3–4.2 GHz), n78 (3.3–3.80 GHz), and n79 (4.4–5.0 GHz) require a wideband coverage extending from 3.3 GHz to at least 5.0 GHz. The proposed antenna covers a high-frequency range from 3.2 to 5.75 GHz. It is fabricated on FR-4 substrate with a dielectric constant of 4.3 to reduce the cost of the antenna with more simplicity in structure. The overall size of the MIMO antenna is 46 mm × 46 mm with a thickness of 1.6 mm. It has a high gain and efficiency of 9 dBi and 90%, respectively. The number of elements can be doubled several times using the same method for mutual coupling reduction. The remainder of the paper is organized as follows. Section II describes the antenna element design and configuration. Section III discusses mutual coupling in MIMO, reduction methods and comparison between these methods with discussions of the experimental and simulated results. MIMO performance is presented in section IV. Finally, Section V presents the conclusion.

II. ANTENNA DESIGN AND CONFIGURATION

The concept of the proposed antenna is based on the use of a rectangular patch antenna with EL slots into the radiating element along with two identical stubs coupled to the partial ground. The antenna is printed on an FR-4 substrate of 4.3 dielectric constant and 0.025 loss tangent (Fig. 1). The center frequency of the designed dipoles is 2.45 GHz. The bandwidth of the antenna is controlled by the width of the patch. Length L and width W of the patch antenna are calculated from Equations (1) to (3). Here, h is the height of FR-4 substrate; ε_{eff}, C, and f_o are the effective permittivity, speed of light (3×10^8 m/s), and center frequency, respectively. Two slots of E and L shapes are etched on the rectangular monopole radiator, which effectively improve the bandwidth ranging from 3.6 to 5.5 GHz by modifying the surface current distribution at higher-order modes. Two protruded stubs are presented at the left and right bottom sections of the monopole. Additional capacitive reactance is mitigated using these two stubs coupled with the partial ground, leading to wider bandwidth ranging from 3.1 to 5.5 GHz. The antenna covers the entire 5G NR sub-6 GHz n77/n78/n79 bands and 5.2 (5.15–5.5) GHz WLAN (Fig. 2).

$$Wp = \frac{c}{4f_o\sqrt{\frac{\varepsilon r+1}{2}}} \tag{1}$$

$$L_{patch} = \frac{c}{4f_o\sqrt{\varepsilon eff}} \tag{2}$$

$$\varepsilon eff = \frac{\varepsilon r+1}{2} + \frac{\varepsilon r-1}{2}\frac{1}{\sqrt{1+12\frac{h}{Wp}}} \tag{3}$$

Table 1 presents the geometric parameters of the antenna. The efficiency and gain of the antenna are 90% and 4 dBi, respectively (Fig. 3 and 4). Figure 5 shows the simulated two-dimensional (2D) radiation pattern at 4.5 GHz with $\theta = 90°$. An omnidirectional radiation pattern in the E-plane is observed.

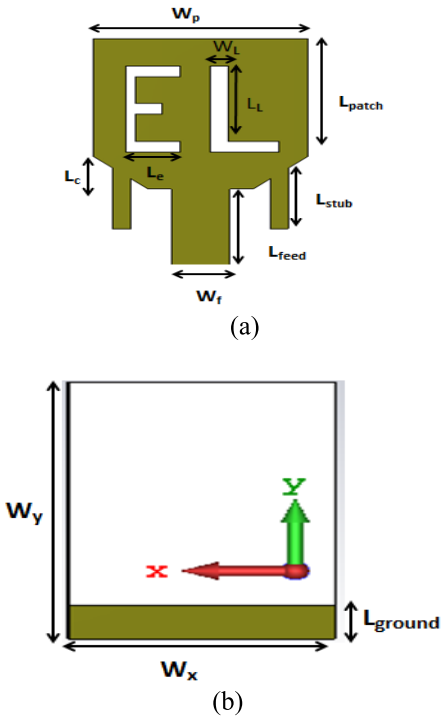

FIGURE 1. Geometry of a single patch antenna. (a) Front side and (b) Backside.

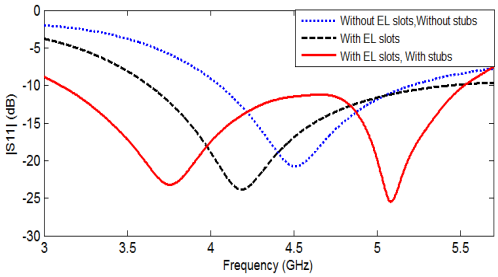

FIGURE 2. Simulated reflection coefficient of a single antenna without EL slots or stubs, with EL slots, and with EL slots and stubs.

TABLE 1. proposed antenna geometric parameters (in Millimeters).

L_{patch}	11	W_p	12	L_{stub}	5.9	L_L	7
L_c	2	L_e	3	L_{feed}	6.6	W_f	3.2
W_L	1	W_x	15	W_y	23	L_{ground}	3

Figure 6 demonstrates the corresponding vector current distribution of the proposed single antenna without and with EL slot. It is visualized that the currents flow in only one direction (Fig. 6 (a)). However, as shown in Figure 6 (b), the currents are densely populated and flowing in different directions. Therefore, merging these currents will widen the bandwidth.

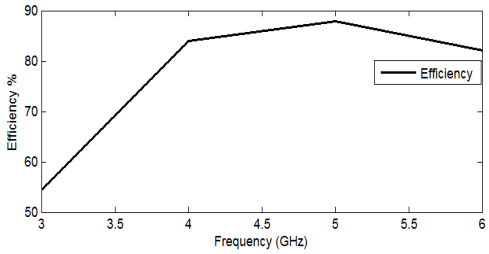

FIGURE 3. Simulated efficiency versus frequency of antenna operation.

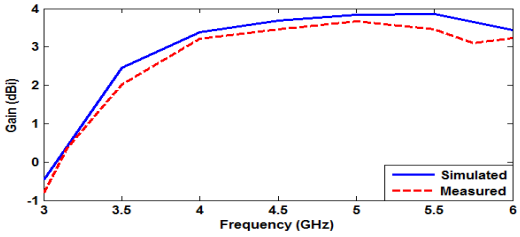

FIGURE 4. Simulated gain over frequency of of antenna operation.

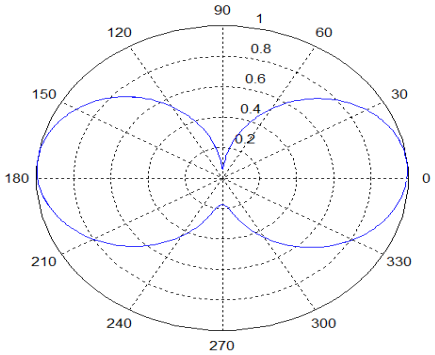

FIGURE 5. Simulated radiation pattern of single element at 4.5 GHz.

III. MUTUAL COUPLING IN MIMO

Mutual coupling is the major issue in designing a MIMO array. Mutual coupling in an array changes the radiation pattern of the array. It is inversely proportional to the spacing between different antenna elements in an array. Thus, several studies employed various methods to solve this problem. For example, in [5], [14], the EBG method was used to reduce mutual coupling. In [7], [9], [13], the DGS method was used to solve this problem. Additionally, some studies used the NL method to solve this problem [15], [16]. In [18], the method of parasitic elements was used. Some authors [10] employed the method of decoupling structure. In this study, we introduce four methods of mutual coupling reduction and compare them to obtain high isolation between ports. These methods are EBG, DGS, capacitive element (CE), and NL.

All the proposed designs of the four-port MIMO array have the same dimensions of 46 mm × 46 mm × 1.6 mm.

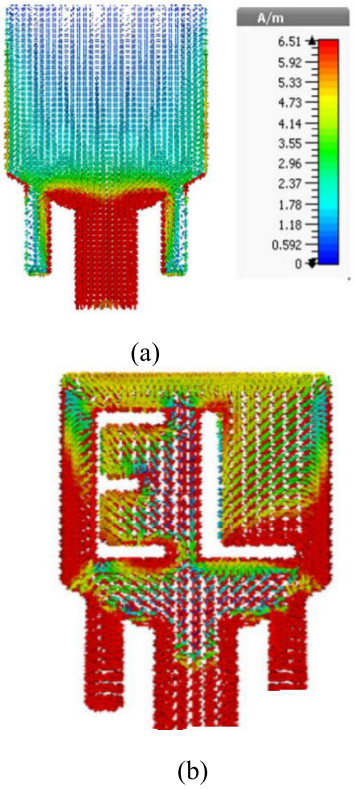

FIGURE 6. Vector current density of reference antenna (a) without EL slot and (b) with EL slot.

A. DESIGN OF FOUR-PORT MIMO ANTENNA ARRAY WITH HIGH ISOLATION BETWEEN PORTS USING THE EBG METHOD

The proposed antenna array is designed on FR-4 substrate of 4.3 dielectric constant and 0.025 loss tangent. The design dimensions are tabulated in Table 2. The antenna array is simulated using the commercial CST 2019 (Fig. 7) and fabricated using the photolithographic process (Fig. 8). The dimensions of the proposed antenna array are 46 mm × 46 mm × 1.6 mm, and center frequency of the designed patch antenna is 2.45 GHz. The spacing between antenna elements is chosen to be 0.3 λ_o according to the parametric study, where λ_o is a free-space wavelength. The antenna array covers the band from 3.2 to 5.75 GHz to serve NR sub-6 GHz (Fig. 9). Figure 10 shows the reflection coefficient at ports 2, 3, and 4. The design is a four-port MIMO antenna array, where the elements are orthogonal to each other to reduce mutual coupling between ports, as shown in Figure 7. The bandwidth ranges from 3.2 to 5.75 GHz at each port. The EBG is introduced (Fig. 7 (c)) in the design to reduce mutual coupling. Figure 11 shows the isolation between ports in the four-port MIMO array without a decoupling network, where poor isolation in the desired band could be noticed. The isolation between ports after inserting EBG reaches a better value greater than −22 dB (Fig. 12).

TABLE 2. proposed antenna geometric parameters (in MILLIMETERS).

Wx	40	W_Y	40	W_4	8.8	g	0.1
W_3	1.2	W_5	0.2	W_6	0.1		

The efficiency and gain are 91% and 9 dBi, respectively (Figs. 13 and 14). The slight variation between the measured and simulated results in the gain and efficiency may be due to the soldering the SMA connector. Meanwhile, the variation is still within the acceptable level. The antenna is an end-fire radiator. The diversity gain (DG) and envelope correlation coefficient (ECC) values reach 10 and less than 0.002, respectively (Figs. 15 and 16). The total active reflection coefficient (TARC) of the MIMO array reaches a value less than −25 dB (Fig. 17).

Figure 7 (d) shows the equivalent circuit of EBG unit cells. Here C1 is the capacitance of the air gap between adjacent EBG unit cells; C2 is the capacitance of the dielectric gap between the top metallic patch and ground plane; L represents the inductance of the metallic vias with radius r. For an EBG structure with patch width W_p, gap width g, substrate thickness h, and dielectric constant ε_r, the values of the inductor L and capacitors (i.e., C1 and C2) are determined using the following equations [23].

$$C1 = \frac{\varepsilon_o Wp}{\pi} \text{arch}\left(\frac{g + Wp}{g}\right) \tag{4}$$

$$C2 = \frac{\varepsilon_o \varepsilon r\, W'}{\pi} \text{arch}\left(\frac{\sinh\left(\pi(W' + g)\right)/4h)}{\sinh(\frac{\pi g}{4h})}\right) \tag{5}$$

$$L = \mu_o h\{\frac{1}{\pi}[ln(\frac{a + \sqrt{a^2 - (2r^2)}}{2r}) + ln2^{0.5}]\} \tag{6}$$

$$F_o = \frac{1}{2\pi\sqrt{LC}} \tag{7}$$

Here, $W' = 1 - 2S/Wp^2 Wp$, $S = \pi r^2$, $a = W + g$, $C = C1 + C2$, and S represents the cross-sectional area of vias hole, $\mu 0$ and ε_o are the permeability and permittivity of free space, respectively.

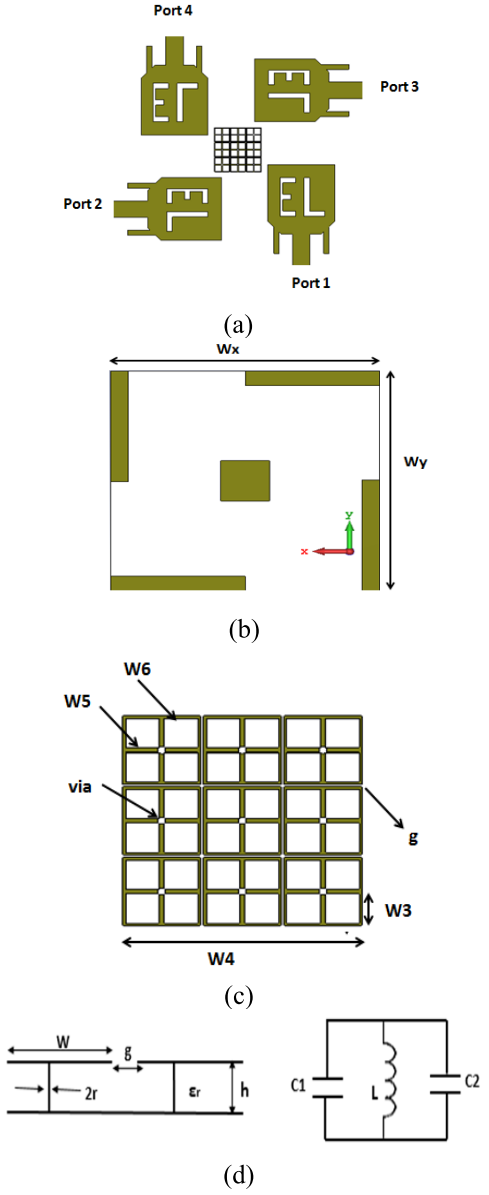

FIGURE 7. Geometry of a 4-port multiple-input multiple-output array. (a) Front side, (b) Backside, (c) Electromagnetic bandgap (EBG) unit cells, and (d) Equivalent circuit of EBG.

B. DESIGN OF THE FOUR-PORT MIMO ANTENNA ARRAY WITH HIGH ISOLATION BETWEEN PORTS USING THE DGS METHOD

The proposed antenna is designed on FR-4 substrate with the same dimensions as the previous design and a square shape with slots etched on the backside of the design (on the ground), as shown in Figure 18. The dimensions of the proposed array are 46 mm × 46 mm × 1.6 mm. The fabricated antenna is shown in Figure 19. The equivalent circuit of the DGS structure is shown in Figure 18 (d). The antenna array covers the band from 3.2 to 5.75 GHz to serve NR sub-6 GHz (Fig. 20). Figure 21 demonstrates the reflection coefficient at ports 2, 3, and 4. The bandwidth at each port ranges from 3.2 to 5.75 GHz. DGS is introduced in the design (Fig. 18 (c)) to reduce mutual coupling, as shown in Figure 22. The dimensions of DGS structure are $W_d = 8.8$, $Wu = 1.2$, $W_b = 0.2$, and $Ws = 0.1$ mm. The isolation between ports is greater than −22 dB (Fig. 21). The efficiency and gain of the four-port MIMO array are 91% and 9 dBi, respectively (Figs. 23 and 24). DG and ECC values reach 10 and less than 0.002, respectively (Figs. 25 and 26). The parameter TARC of the MIMO array is less than −25 dB (Fig. 27).

C. DESIGN OF THE FOUR-PORT MIMO ANTENNA ARRAY WITH HIGH ISOLATION BETWEEN PORTS USING THE NL METHOD

Figure 28 demonstrates the proposed antenna array using the NL method with dimensions of $w = 1$, $R = 3$, and $Ln =$

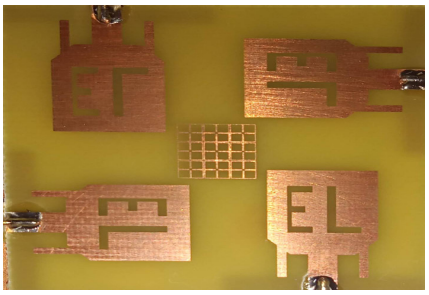

(a)

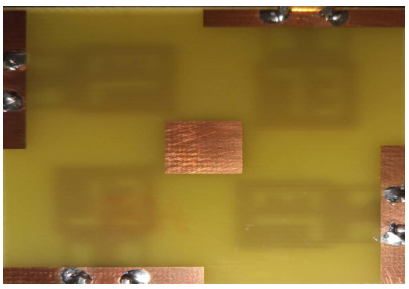

(b)

FIGURE 8. Fabrication of the proposed antenna (a) Front side (b) Back side.

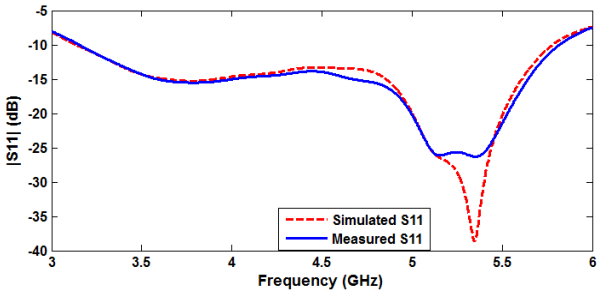

FIGURE 9. Simulated and measured reflection coefficient at port 1.

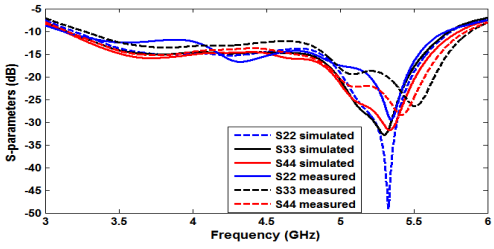

FIGURE 10. Simulated and measured return loss at ports 2, 3, and 4.

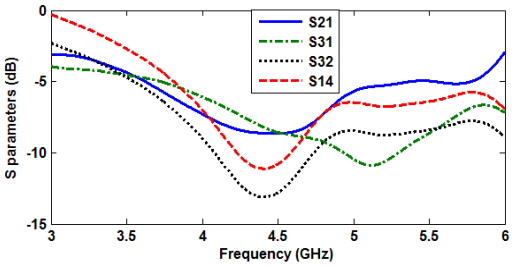

FIGURE 11. Simulated and measured isolation between ports without) electromagnetic bandgap.

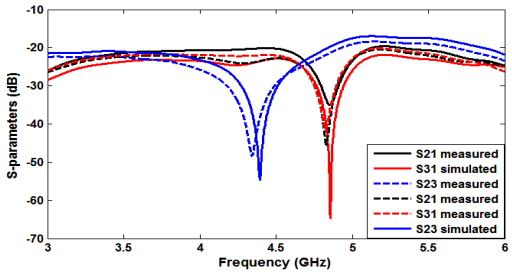

FIGURE 12. Simulated and measured isolation between ports.

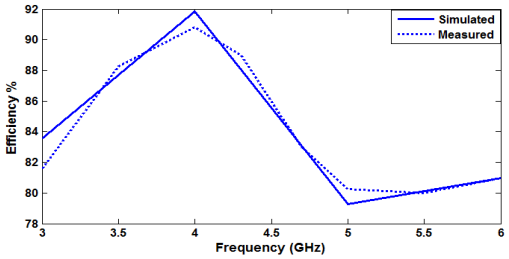

FIGURE 13. Simulated and measured efficiency of the four-port multiple-input multiple-output array.

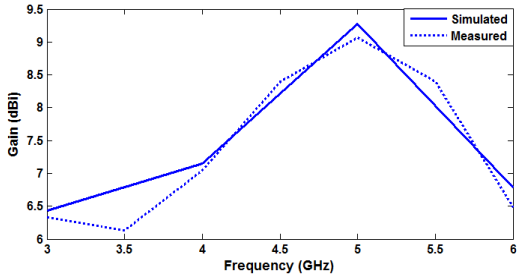

FIGURE 14. Simulated and measured gain over frequency for the four-port multiple-input multiple-output array.

20 mm. The dimensions of the proposed array are 46 mm × 46 mm × 1.6 mm. The equivalent circuit of this antenna is shown in Figure 28 (c), and the fabricated antenna is shown in Figure 29. The equivalent circuit is signified by inductance (L), resistance (R), and capacitance (C). C and L are responsible for electric and magnetic coupling between the antenna elements, respectively. The antenna array covers the band from 3.2 to 5.75 GHz to serve NR sub-6 GHz (Fig. 30).

The reflection coefficients at ports 2, 3, and 4 are illustrated in Fig. 31. The NL method can generate enough decoupling current that improves isolation to −20 dB (Fig. 32). The efficiency fluctuates around 90%, while the gain ranges from 6 to 9 dBi (Figs. 33 and 34). DG and ECC are about 10 and less than 0.003, respectively, as shown in Figures 35 and 36. The parameter TARC of the MIMO array is less than −25dB

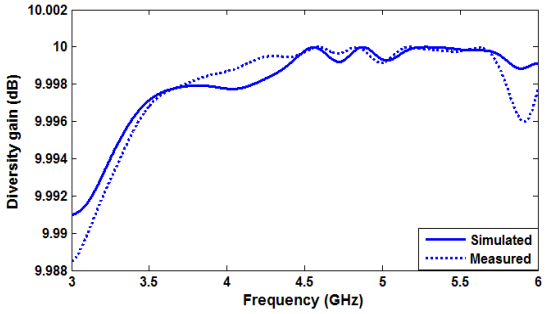

FIGURE 15. Simulated diversity gain over frequency for the four-port multiple-input multiple-output array.

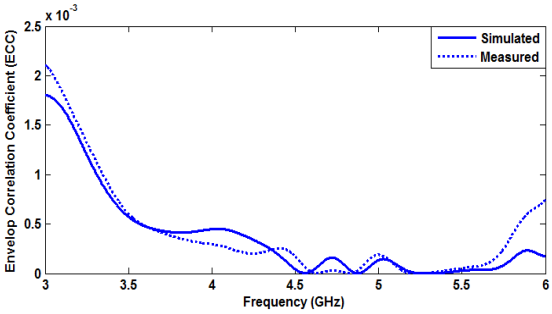

FIGURE 16. Simulated and measured envelope correlation coefficient over frequency for the four-port multiple-input multiple-output array.

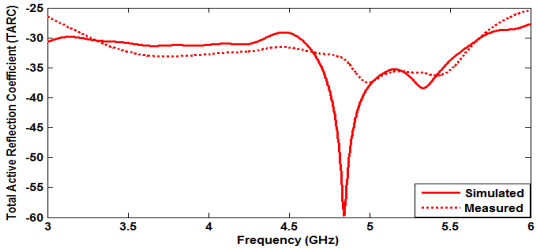

FIGURE 17. Simulated and measured total active reflection coefficient over frequency for the four-port multiple-input multiple-output array.

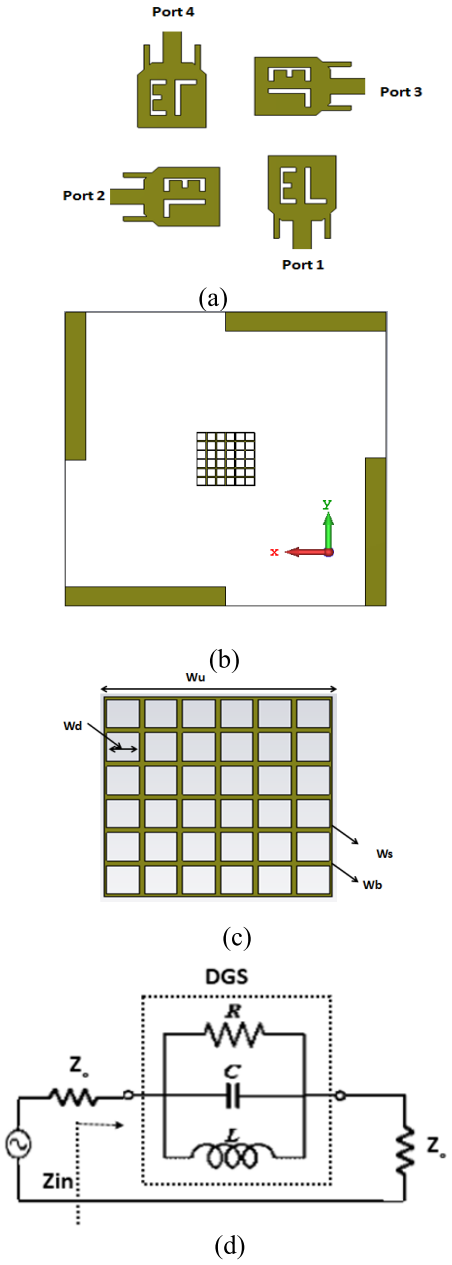

FIGURE 18. Geometry of a four-port multiple-input multiple-output array. (a) Front side, (b) Backside, (c) Defected ground structure (DGS) unit cells, and (d) Equivalent circuit of DGS.

(Fig. 37). Figure 38 shows the surface current distributions to further verify the effect of the decoupling structure on the antenna performance. After inserting the decoupling structure, the current is mainly concentrated near the horizontal circular inductive line, providing high inductive impedance. Almost zero current is induced in the other antenna elements, which is the reason of reducing the mutual coupling.

D. DESIGN OF A FOUR-PORT MIMO ANTENNA ARRAY WITH A HIGH ISOLATION BETWEEN PORTS USING THE CE METHOD

In this design using the CE method, the horizontal and vertical parasitic elements are introduced at the bottom side of the antennas, as shown in Figure 39. The dimensions of the proposed array are 46 mm × 46 mm × 1.6 mm. The fabricated antenna is shown in Fig. 40. The antenna array covers the band from 3.2 to 5.75 GHz to serve NR sub-6 GHz (Fig. 41). Figure 42 demonstrates the reflection coefficient at ports 2, 3, and 4. Since the gap between the antennas is small, the space and surface waves enhance the mutual coupling. The introduced parasitic elements with dimensions of $Lc_1 = 6$, $Lc_2 = 7$, $Lc_3 = 3$, $Lc_4 = 9$, and $W_a = 2$ mm capture these waves and convert them into surface currents, reducing mutual coupling (Fig. 43). The efficiency fluctuates around 90%, while the gain ranges from 9 to 9.5 dBi (Figs. 44 and 45). DG and ECC are about 10 and less than 0.003, respectively, as shown in Figures 46 and 47. The

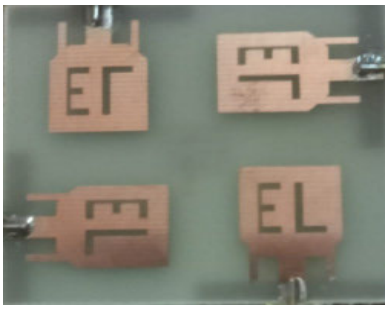

(a)

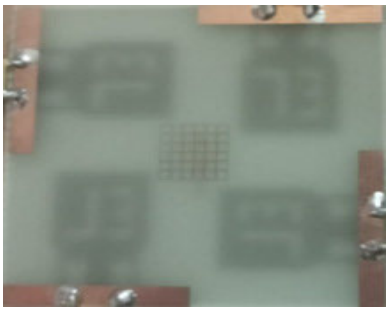

(b)

FIGURE 19. Fabrication of the proposed antenna (a) Front side and (b) Back side.

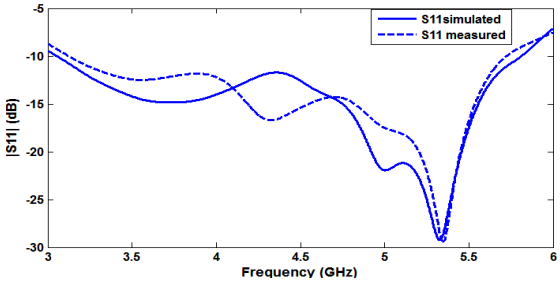

FIGURE 20. Simulated and measured reflection coefficient.

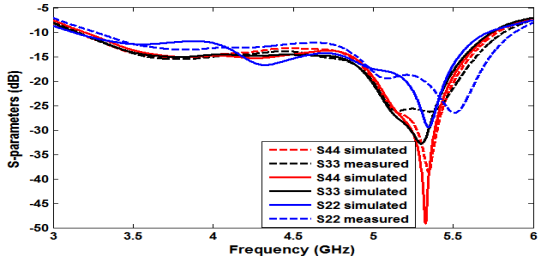

FIGURE 21. Simulated and measured return loss at port 2, 3, and 4.

parameter TARC of the MIMO array has a value less than −25 dB (Fig. 48).

IV. MIMO ANTENNA PERFORMANCE

Several parameters are used to study the performance of the MIMO antenna. One of the main dynamic parameters for estimating the performance of the MIMO antenna is ECC.

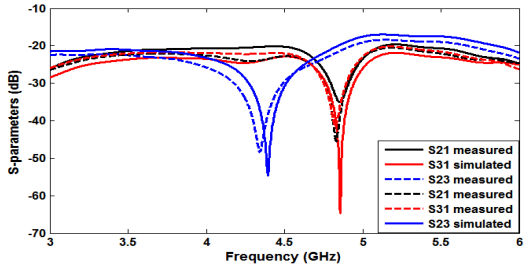

FIGURE 22. Simulated and measured isolation between ports.

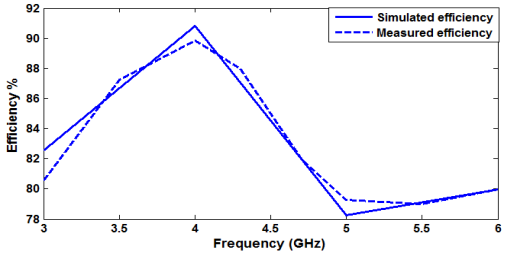

FIGURE 23. Simulated and measured efficiency of the four-port multiple-input multiple-output array.

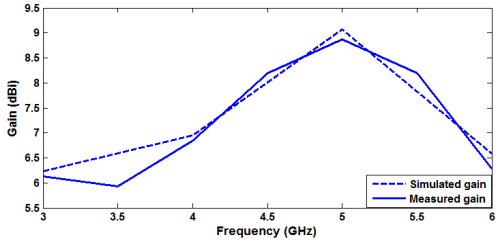

FIGURE 24. Simulated and measured gain over frequency of the four-port multiple-input multiple-output array.

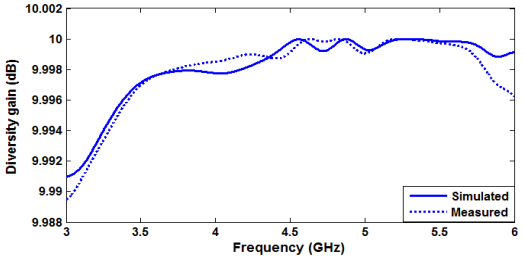

FIGURE 25. Simulated diversity gain over frequency for the four-port multiple-input multiple-output array.

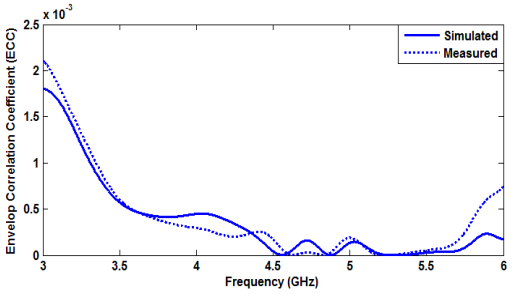

FIGURE 26. Simulated and measured envelop correlation coefficient over frequency for the four-port multiple-input multiple-output array.

ECC is one of the key performance metrics of the MIMO antenna system. It can be calculated from the S-parameters

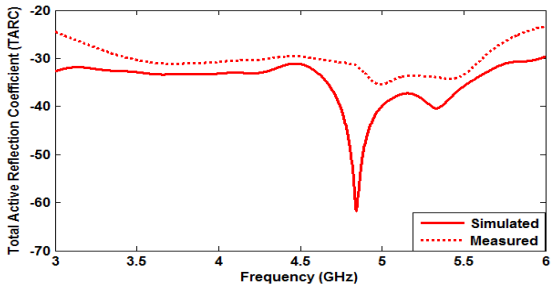

FIGURE 27. Simulated and measured total active reflection coefficient over frequency for the four-port multiple-input multiple-output array.

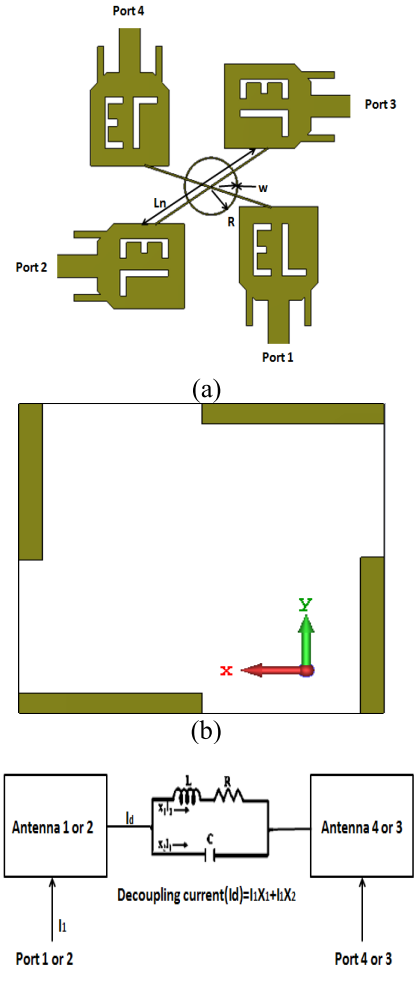

FIGURE 28. Geometry of a four-port multiple-input multiple-output array. (a) Front side, (b) Backside, and (c) Equivalent circuit model of the proposed multiple-input multiple-output antenna.

using the following equation [24]

$$\mathrm{ECC} = |Sii * Sij + Sji * Sjj|^2/(1 - |Sii|^2 - |Sji|^2) * (1 - |Sjj|^2 - |Sij|^2) \quad (8)$$

The results of ECC in the four methods are approximately 0.002.

DG is the loss in transmission power when the diversity mechanism is performed on the MIMO system.

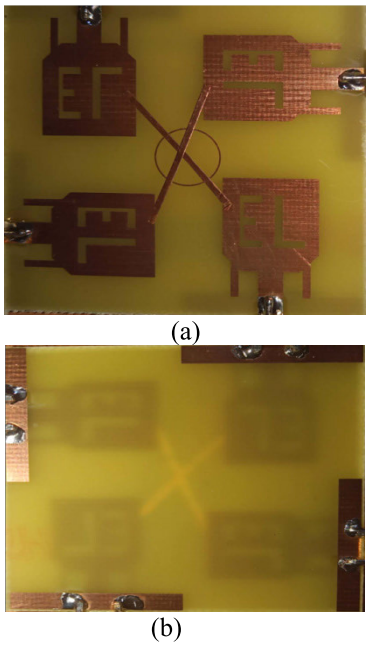

FIGURE 29. Fabricated proposed antenna(a) Front side and (b) Back side.

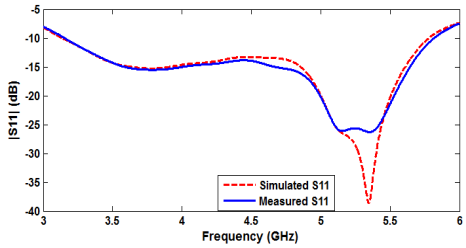

FIGURE 30. Simulated and measured reflection coefficient at port 1.

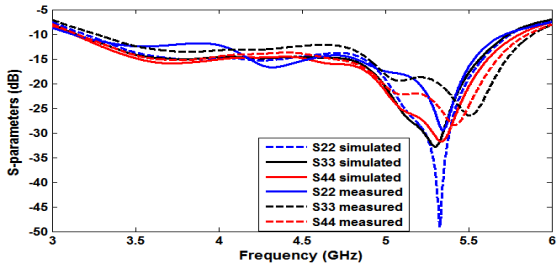

FIGURE 31. Simulated and measured return loss at ports 2, 3, and 4.

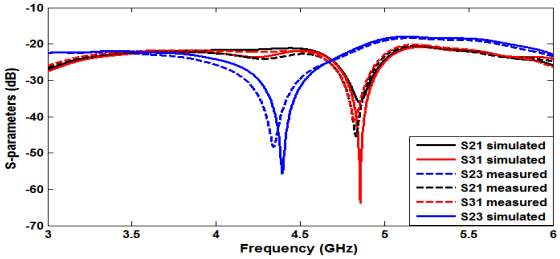

FIGURE 32. Simulated and measured isolation between ports.

DG is calculated using the following equation [24].

$$\mathrm{DG} = 10\sqrt{1 - (\mathrm{ECC})^2} \quad (9)$$

DG is approximately 10 dB (Figs. 15, 25, 35, and 46).

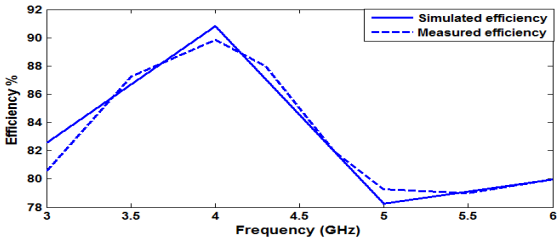

FIGURE 33. Simulated and measured efficiency of a four-port multiple-input multiple-output array.

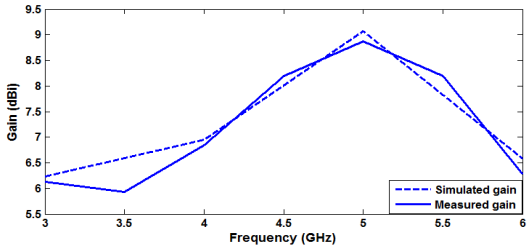

FIGURE 34. Simulated and measured gain over frequency of a four-port multiple-input multiple-output array.

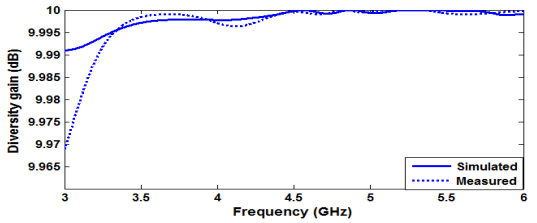

FIGURE 35. Simulated and measured diversity gain over frequency for a four-port multiple-input multiple-output array.

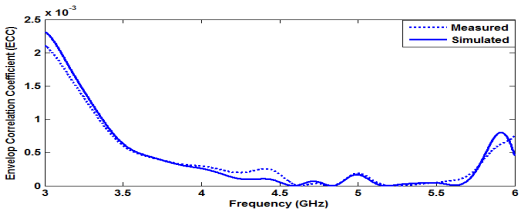

FIGURE 36. Simulated and measured envelop correlation coefficient over frequency for a four-port multiple-input multiple-output array.

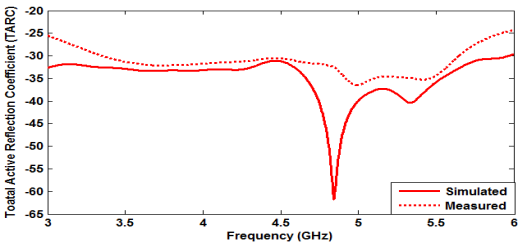

FIGURE 37. Simulated and measured total active reflection coefficient over frequency for a four-port multiple-input multiple-output array.

The third parameter that qualifies the coupling among ports is TARC. TARC is a parameter used to validate the performance of a MIMO antenna. TARC expresses the total incident power to the radiated power of the MIMO antenna array.

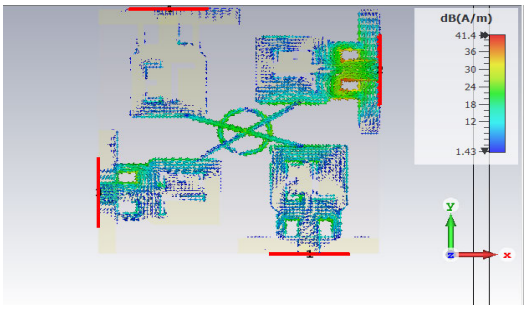

FIGURE 38. Surface current at 4.5 GHz when port 2 is on.

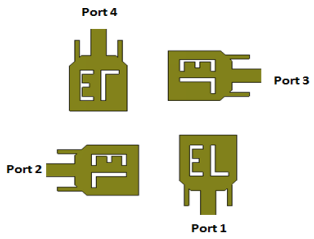

(a)

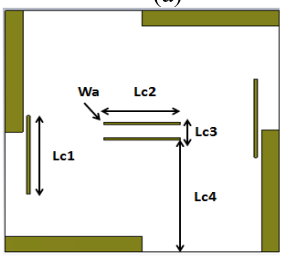

(b)

FIGURE 39. Geometry of a four-port multiple-input multiple-output array. (a) Front side and (b) Backside.

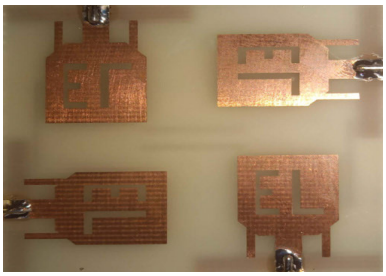

(a)

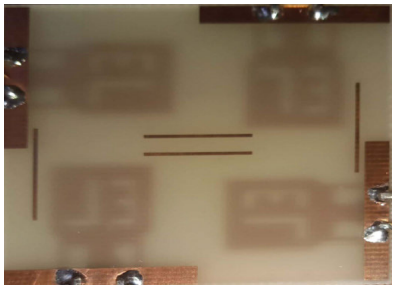

(b)

FIGURE 40. Fabricated antenna array based on the capacitive element method. (a) Front side and (b) Back side.

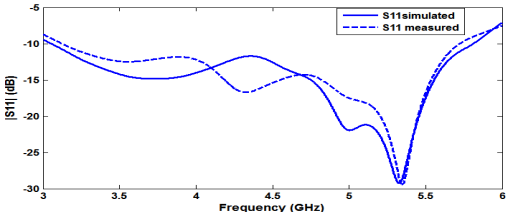

FIGURE 41. Simulated and measured reflection coefficient at port 1.

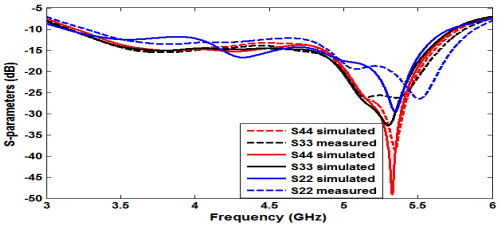

FIGURE 42. Simulated and measured return loss at port 2, 3, and 4.

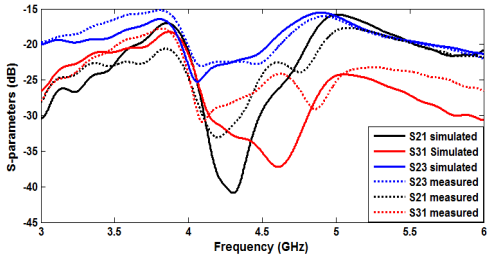

FIGURE 43. Simulated and measured isolation between ports.

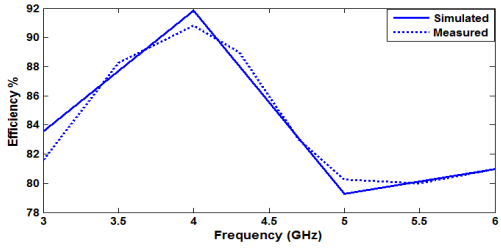

FIGURE 44. Simulated and measured efficiency of a four-port multiple-input multiple-output array.

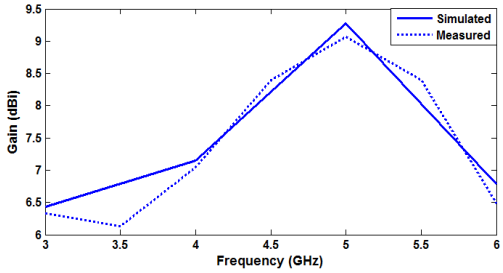

FIGURE 45. Simulated and measured gain over frequency of a four-port multiple-input multiple-output array.

TARC can be calculated using the following equation:

$$\Gamma = \frac{\sqrt{\left(|\mathrm{Sii} + \mathrm{Sij}e^{j\circ|2}\right) + \left(|\mathrm{Sji} + \mathrm{Sjj}e^{j\circ|2}\right)}}{\sqrt{2}} \qquad (10)$$

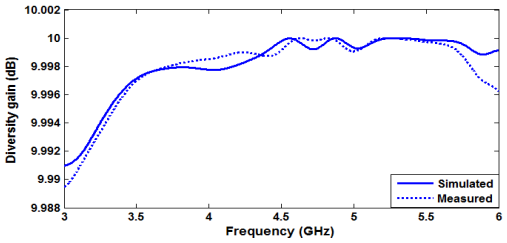

FIGURE 46. Simulated and measured diversity gain over frequency for a four-port multiple-input multiple-output array.

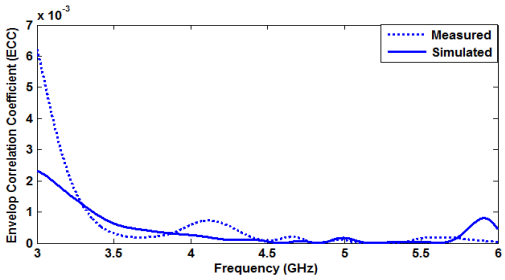

FIGURE 47. Simulated and measured envelop correlation coefficient over frequency for a four-port multiple-input multiple-output array.

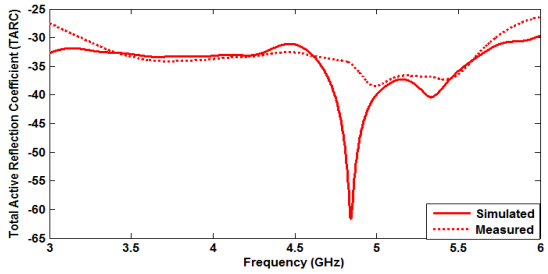

FIGURE 48. Simulated and measured total active reflection coefficient over frequency for a four-port multiple-input multiple-output array.

Here, θ is the input phase angle ranging from 0° to 180° with step increment of 30°; Sii and Sjj are the reflection coefficients of ports 1 and 2, respectively. TARC is shown in Figures 17, 27, 37, and 48 for all methods.

The fourth parameter is mean effective gain (MEG), MEG accounts for total efficiency, gain, and measuring the antenna–channel mismatch. MEG1 for first antenna/ MEG2 for second antenna and MEG3 for the third antenna/MEG4 for the fourth antenna range from 0.966 to 1.0067. MEG for each antenna ranges from −5.6 to −6.4 dB, as presented in Table 5. The MEG is calculated using the following equation

$$\mathrm{MEG}i = 0.5\eta irad = 0.5(1 - \sum_{j=1}^{k} |Sij|^2) \qquad (11)$$

where K is the number of antennas; in the case of 4, i is the active antenna, and $\eta irad$ is the radiation efficiency of i th antenna.

$$\mathrm{MEG1} = 0.5(1—|S11|^2—|S12|^2—|S13|^2—|S14|^2)$$
$$\mathrm{MEG2} = 0.5(1—|S21|^2—|S22|^2—|S23|^2—|S24|^2)$$

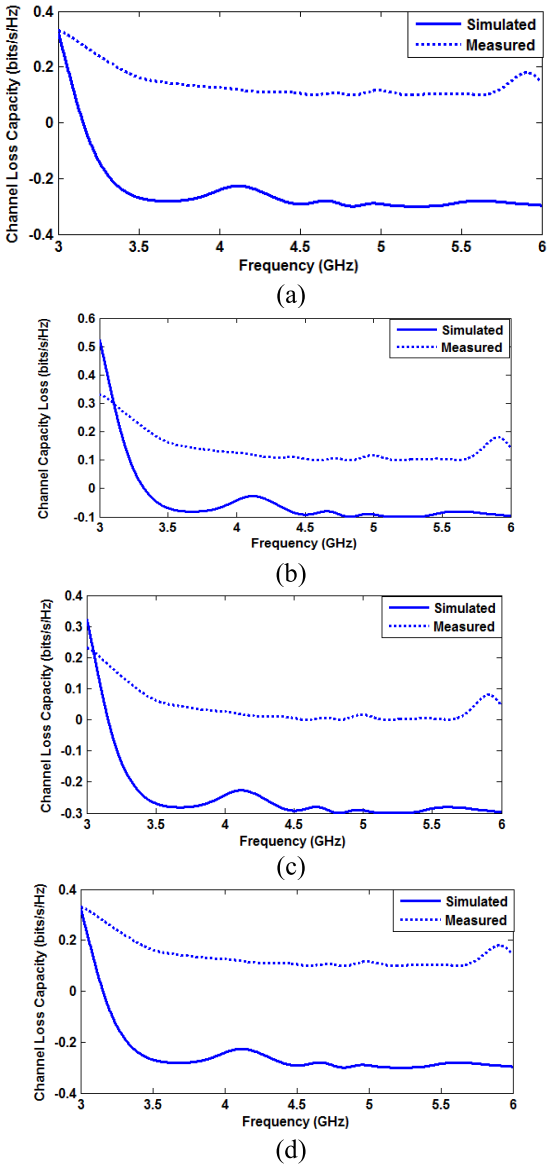

FIGURE 49. SChannel Capacity Loss of the proposed four-port multiple-input multiple-output antenna using (a) Electromagnetic bandgap, (b) Defected ground structure, (c) Neutralization line, and (d) Capacitive element.

$$\text{MEG3} = 0.5(1—|S31|^2—|S32|^2—|S33|^2—|S34|^2)$$
$$\text{MEG4} = 0.5(1—|S41|^2—|S42|^2—|S43|^2—|S44|^2)$$

The MEG values should be between

$$-3 \leq \text{MEG (dB)} < -12$$

The fifth parameter is Channel Capacity Loss (CCL), CCL is one of the fundamental metrics among the MIMO performance parameters. CCL is calculated using the following equation:

$$C\ loss = -log_2(\Psi^R) \quad (12)$$

TABLE 3. Comparison between the four methods of reducing mutual coupling in Mean effective gain at different frequencies.

		Methods			
Freq. GHz	MEG	EBG	DGS	NL	CE
3.5	MEG1(dB)	−6.2330	−6.33	−6.3446	−6.0695
	MEG2	−6.2510	−6.3469	−6.4107	−6.0599
	MEG3	−5.8020	−5.638	−5.5585	−5.9181
	MEG4	−5.8270	−5.7456	−5.6718	−5.9759
	MEG1/MEG2	1.0021	1.0020	1.0076	0.9989
	MEG3/MEG4	1.0029	1.0125	1.0131	1.0067
4.5	MEG1	−6.4146	−6.4946	−6.5219	−6.3145
	MEG2	−6.2848	−6.3689	−6.4577	−6.0146
	MEG3	−5.7243	−5.6380	−5.4971	−5.9766
	MEG4	−5.7646	−5.6941	−5.5894	−5.9025
	MEG1/MEG2	0.9852	0.9856	0.9926	0.9661
	MEG3/MEG4	1.0046	1.0065	1.0107	0.9915
5.5	MEG1	−5.8559	−5.7128	−5.8290	−5.6596
	MEG2	−5.8741	−5.7707	−5.7442	−5.6758
	MEG3	−6.1514	−6.3005	−6.2913	−6.4372
	MEG4	−6.2298	−6.3203	−6.1740	−6.4274
	MEG1/MEG2	1.0021	1.0067	0.9903	1.0019
	MEG3/MEG4	1.0091	1.0023	0.9866	0.9989

TABLE 4. Comparison between electromagnetic band gap, defected ground structure, Neutralization line, AND capacitive element in THE FOUR-port multiple-input multiple-output antenna array.

	Methods			
Parameter	EBG	DGS	NL	CE
Isolation improvement (dB)	<−20: −65	<−19: −60	<−20: −55	<−15:−40
DG	9.996	9.998	9.999	9.994
ECC	<0.002	<0.015	<0.002	< 0.
Average MEG for each port (dB)	−5.724	−5.638	−5.4971	−5.9766
TARC (dB)	<−26	<−24	<−25	<−30
Gain (dBi)	9	8.9	8.7	9
Efficiency	92%	90%	88%	91%

Here, Ψ^R is the correlation matrix of the receiving antenna, which is expressed as follows:

$$\Psi R = \begin{matrix} \Psi ii & \Psi ij \\ \Psi ji & \Psi jj \end{matrix}$$

Here, $\Psi ii = 1—(|Sii|^2 + |Sij|^2)$, $\Psi ij = -(Sii * Sij + Sji * \Psi jj)$, $\Psi ji = -(Sjj * Sji + Sij * Sii)$, $\Psi jj = 1—(|Sjj|2 + |Sji|^2)$.

The desired value of CCL is less than 0.4 bits/s/Hz. In our designs, CCL is less than this value; thus, it is satisfied. The results of CCL are shown in Fig. 49.

Figure 50 shows the radiation pattern in the E-plane at a frequency of 4.5 GHz. The main lobe is directed at $\theta = 90°$, and is perpendicular to each other, as shown in Figure 50 (a), (b), (c), and (d). The E-plane patterns are 90° out of phase. Similarly, the E-plane patterns are similar

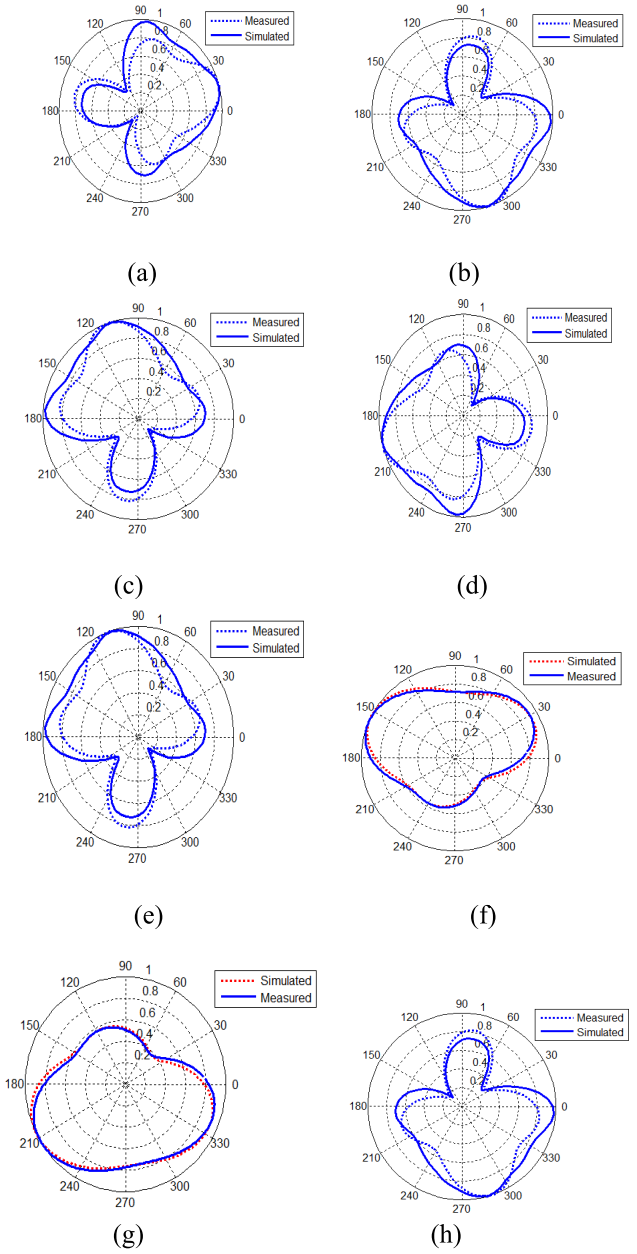

FIGURE 50. Measured and Simulated radiation pattern at $\theta = 90°$ at frequency of 4.5GHz (a) at port 1 (b) at port 2 (c) at port 3 (d) at port 4. At $\Phi = 0°$ at frequency of 4.5GHz (d) at port 1 (e) at port 2 (f) at port 3 (g) at port 4.

between antennas, whereas the H-plane patterns are 180° out of phase between antennas 2 and 3 and between antennas 1 and 4, as shown in Figure 50 (e), (f), (g) and (h). This proves that the proposed antenna achieves pattern diversity, which ensures that there is no interference during the reception and maintains an omnidirectional radiation pattern in E-plane and H-plane. The radiation pattern was measured in the Science and Technology Center of Excellence, Egypt, using a compact multiprobe antenna test station (STARLAB-18), VNA model: Agilent E8363B (10 MHz–40 GHz). The equivalent circuit of the antenna array is shown in Figure 51.

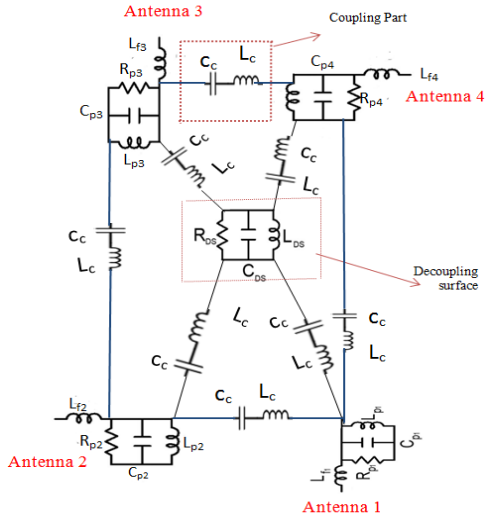

FIGURE 51. Equivalent circuit of the four-port multiple-input multiple-output antenna array with decoupling surface.

V. COMPARISON BETWEEN EBG, DGS, NL, AND CE BASED DESIGNS

Table 4 compares the results of the four methods of reducing mutual coupling between antenna elements. All methods of reducing mutual coupling achieve high isolation between ports and give satisfied MEG, CCL, TARC, DG, and ECC. The EBG and DGS methods are the best in isolation reduction. This is due to the presence of gaps between each unit and adjacent unit cells in the nine-unit cells in addition to the capacitance obtained from the dielectric gap between the top metallic patch and ground plane (Fig. 7 (c)). This adds extra capacitance that makes more isolation between antenna elements, as shown in the equivalent circuit in Figure 7 (d). In the EBG method, the isolation is less than −22 dB, reaching −65 dB with DG, TARC, and ECC approaching 9.996, less than −25 dB, and 0.015, respectively. However, in the DGS method, the isolation is less than −19 dB, reaching −60 dB with DG, TARC, and ECC approaching 9.998, less than −30 dB, and less than 0.002, respectively. Meanwhile, the NL and CE methods are less in isolation than the first two methods. In the NL method, there is one capacitance, as shown in Figure 28 (c). The NL method can generate a sufficient amount of decoupling current and improve isolation, (Fig. 28 (c)) as the isolation reaches −20 to −55 dB with DG, TARC, and ECC approaching 9.99, less than −30 dB, and less than 0.002, respectively. However, in the CE method, there are capacitances resulting from the four transmission lines found at the bottom side of the antennas (parasitic elements) that are less effective in isolation, as the isolation approaches −15 dB to −40 dB with DG, TARC, and ECC approach to 9.994, less than −30 dB, and less than 0.004, respectively. Therefore, the best method is EBG because it has high isolation due to extra capacitance in the circuit, high DG, and high efficiency (i.e., 92%), In addition, gain approaches 9 dBi.

TABLE 5. Performance comparison between the proposed design and previous studies.

Ref	No of ports	Substrate	Decoupling method	Isolation improvement (dB)	Design complexity	BW GHz	Size mm^3	DG	ECC	Gain dBi	Efficiency %
[5]	4	FR4	EBG	−17.5	Easy	4:5.2	60 × 60 × 1.6	4.4:10	≤0.2	8	90
[7]	2	FR4	DGS	−14	Easy	2.2:6.28	45 × 45 × 1.6	Not found	≤0.25	4	91
[8]	4	FR4	planar H-shaped Decoupling structure	−14	medium	5.2:5.8	42 × 42 × 0.8	Not found	Not found	5	80
[9]	4	FR4	DGS	−10	Easy	3.2:5.7	40 × 30 × 1.6	9.98	<0.05	3.5	82
[10]	4	FR4	L-Shaped Decoupling structure	−15	Medium	4.58:6.12	30 × 30 × 0.8	9.85	<0.15	4.02	67–82
[11]	8	FR4	Grounding branch	−15	Medium	2.4:2.7 3.3:3.7	124 × 74 × 4	Not found	<0.21	Not found	60:80
[12]	5	Rogers/duroid 5880	X-shaped strip	−10	Difficult	5.6	152 × 50 × 1	Not found	Not found	13.6	Not found
[13]	2	FR4	Hybrid(DGS)	−12.2	Difficult	4.7:10.6	45 × 59.6 × 0.5	Not found	Not found	8	Not found
[14]	2	jean's	Metamaterial(EBG)	−10	Medium	1.34: 3.92 4.34:6.34	100 × 60 × 1	>9	<0.04	3:5	Not found
[15]	4	FR4	naturalization lines	−20.55	Easy	2.09:2.68 4.73:6.33	45 × 60 × 1.6	9.9	<0.05	Not found	Not found
[16]	2	FR4	naturalization lines	−22	Easy	3.1:5	35 × 33 × 0.8	Not found	<0.1	5	80
[17]	4	RO4350 B	double-layer metasurface	−25	Difficult	5.8	110 × 110 × 1.52	Not found	<0.12	5	77
[18]	2	Rogers TMM4	parasitic elements	−15	Easy	3:8.5	40.5 × 26 × 1.524	Not found	<0.6	5.75	85
Proposed design	4	FR4	DGS-EBG-naturalization lines-parasitic elements	−22	Easy	3.2:5.75	40 × 40 × 1.6	>9.9	<0.05	9	91

Here, cp1 = cp2 = cp3 = c for patch antenna $+C_{stubs}L_{p1} = L_{p2} + L_{p3}$, $R_{p1} + R_{p2} + R_{p3} = 50\Omega$.

VI. CONCLUSION

In this study, a four-port MIMO array with high isolation between ports is introduced. We introduce four methods of reducing mutual coupling and compare the performances of each method. The prototype of the antenna element with optimized dimensions has been simulated using CST STUDIO SUITE ver. 2019. The antenna arrays are designed on an FR-4 substrate with a noticeable cost reduction. We found that the simulated and measured results are consistent. The antenna operates in the band from 3.2 to 5.75 GHz to serve in 5G NR sub-6 GHz n77/n78/n79 and 5 GHz WLAN. It shows good results of MEG less than −6 Db. In addition, TARC is less than −20 Db; ECC is less than 0.002; DG approaches 10 dB; and CCL is less than 0.4 bits/s/Hz. The four methods used to reduce the mutual coupling between antennas are EBG, DGS, NL, and CE. The best method is EBG because it has high isolation due to extra capacitance in the circuit, high DG, high efficiency (i.e., 92%), and gain of 9 dBi. Table 5 summarizes the characteristics of the proposed antenna compared to previous antennas discussed in the literature.

REFERENCES

[1] R. He, B. Ai, G. L. Stüber, G. Wang, and Z. Zhong, "Geometrical-based modeling for millimeter-wave MIMO mobile-to-mobile channels," *IEEE Trans. Veh. Technol.*, vol. 67, no. 4, pp. 2848–2863, Apr. 2018.

[2] K. Guan, Z. Zhong, J. I. Alonso, and C. Briso-Rodriguez, "Measurement of distributed antenna systems at 2.4 GHz in a realistic subway tunnel environment," *IEEE Trans. Veh. Technol.*, vol. 61, no. 2, pp. 834–837, Feb. 2012.

[3] M. Li, X. Chen, A. Zhang, and A. A. Kishk, "Dual-polarized broadband base station antenna backed with dielectric cavity for 5G communications," *IEEE Antennas Wireless Propag. Lett.*, vol. 18, no. 10, pp. 2051–2055, Oct. 2019.

[4] *Federal Communications Commission Revision of Part 15 of the Commision's Rules Regarding Ultra-Wideband Transmission System from 3.1 to 10.6 GHz, ET-Docket*, Federal Communications Commision, Washington, DC, USA, 2002.

[5] W. Wu, B. Yuan, and A. Wu, "A quad-element UWB-MIMO antenna with band-notch and reduced mutual coupling based on EBG structures," *Int. J. Antennas Propag.*, vol. 2018, Feb. 2018, Art. no. 8490740.

[6] G. Dubost and A. Rabbaa, "Analysis of a slot microstrip antenna," *IEEE Trans. Antennas Propag.*, vol. 34, no. 2, pp. 155–163, Feb. 1986.

[7] R. Anitha, P. V. Vinesh, K. C. Prakash, P. Mohanan, and K. Vasudevan, "A compact quad element slotted ground wideband antenna for MIMO applications," *IEEE Trans. Antennas Propag.*, vol. 64, no. 10, pp. 4550–4553, Oct. 2016.

[8] Y. Luo, Q.-X. Chu, J.-F. Li, and Y.-T. Wu, "A planar H-shaped directive antenna and its application in compact MIMO antenna," *IEEE Trans. Antennas Propag.*, vol. 61, no. 9, pp. 4810–4814, Sep. 2013.

[9] J. Kulkarni, A. Desai, and C.-Y.-D. Sim, "Wideband four-port MIMO antenna array with high isolation for future wireless systems," *AEU-Int. J. Electron. Commun.*, vol. 128, Jan. 2021, Art. no. 153507, doi: 10.1016/j.aeue.2020.153507.

[10] M. Yang and J. Zhou, "A compact pattern diversity MIMO antenna with enhanced bandwidth and high-isolation characteristics for WLAN/5G/WiFi applications," *Microw. Opt. Technol. Lett.*, vol. 62, no. 6, pp. 2353–2364, 2020.

[11] W. Jiang, Y. Cui, B. Liu, W. Hu, and Y. Xi, "A dual-band MIMO antenna with enhanced isolation for 5G smartphone applications," *IEEE Access*, vol. 7, pp. 112554–112563, 2019.

[12] X. J. Zou, G. M. Wang, Y. W. Wang, and H. P. Li, "Decoupling antenna array with X-shaped strip," *Int. J. RF Microw. Comput.-Aided Eng.*, vol. 29, no. 4, pp. 1–7, Apr. 2018.

[13] X.-J. Zou, G.-M. Wang, Y.-W. Wang, and B.-F. Zong, "Mutual coupling reduction of quasi-yagi antenna array with hybrid wideband decoupling structure," *AEU-Int. J. Electron. Commun.*, vol. 129, Feb. 2021, Art. no. 153553.

[14] S. Roy and U. Chakraborty, "Mutual coupling reduction in a multi-band MIMO antenna using meta-inspired decoupling network," *Wireless Pers. Commun.*, vol. 114, no. 4, pp. 3231–3246, Oct. 2020.

[15] A. Birwal, S. Singh, B. K. Kanaujia, and S. Kumar, "MIMO/diversity antenna with neutralization line for WLAN applications," *MAPAN*, vol. 36, pp. 763–772, Jan. 2021.

[16] S. Zhang and G. F. Pedersen, "Mutual coupling reduction for UWB MIMO antennas with a wideband neutralization line," *IEEE Antennas Wireless Propag. Lett.*, vol. 15, pp. 166–169, 2016.

[17] J. Tang, F. Faraz, X. Chen, Q. Zhang, Q. Li, Y. Li, and S. Zhang, "A metasurface superstrate for mutual coupling reduction of large antenna arrays," *IEEE Access*, vol. 8, pp. 126859–126867, 2020.

[18] M. S. Khan, A.-D. Capobianco, M. F. Shafique, B. Ijaz, A. Naqvi, and B. D. Braaten, "Isolation enhancement of a wideband MIMO antenna using floating parasitic elements," *Microw. Opt. Technol. Lett.*, vol. 57, no. 7, pp. 1677–1682, 2015.

[19] A. A. Althuwayb, "Low-interacted multiple antenna systems based on metasurface-inspired isolation approach for MIMO applications," *Arabian J. Sci. Eng.*, pp. 1–10, 2021, doi: 10.1007/s13369-021-05720-6.

[20] H.-X. Xu, G.-M. Wang, and M.-Q. Qi, "Hilbert-shaped magnetic waveguided metamaterials for electromagnetic coupling reduction of microstrip antenna array," *IEEE Trans. Magn.*, vol. 49, no. 4, pp. 1526–1529, Apr. 2013.

[21] T. Shabbir, R. Saleem, S. S. Al-Bawri, M. F. Shafique, and M. T. Islam, "Eight-port metamaterial loaded UWB-MIMO antenna system for 3D system-in-package applications," *IEEE Access*, vol. 8, pp. 106982–106992, 2020.

[22] S. Sharma, B. K. Kanaujia, and M. K. Khandelwal, "Implementation of four-port MIMO diversity microstrip antenna with suppressed mutual coupling and cross-polarized radiations," *Microsyst. Technol.*, vol. 26, pp. 993–1000, Aug. 2019, doi: 10.1007/s00542-019-04574-1.

[23] K. Ding, C. Gao, D. Qu, and Q. Yin, "Compact broadband MIMO antenna with parasitic strip," *IEEE Antennas Wireless Propag. Lett.*, vol. 16, pp. 2349–2353, 2017.

[24] K. S. Sultan and H. H. Abdullah, "Planar UWB MIMO-diversity antenna with dual notch characteristics," *Prog. Electromagn. Res. C*, vol. 93, pp. 119–129, 2019.

AMANY A. MEGAHED graduated from the Department of Communication and Electronics Engineering, Faculty of Engineering, Mansoura University, in 2011. She received the master's degree in engineering from the Faculty of Engineering, Mansoura University, in 2019. She currently works as an Assistant Teacher at the Higher Institute of Engineering and Technology, New Damietta.

MOHAMED ABDELAZIM received the B.Sc., M.Sc., and Ph.D. degrees in communication engineering from Mansoura University, Egypt, in 1995, 2001, and 2006, respectively. He worked as the CIO with Mansoura University. Since 2019, he has been the Dean of the Faculty of Engineering. He is currently a Full Professor with the Faculty of Engineering, Mansoura University. His research interests include wireless telecommunication systems as 3G, 4G, and 5G mobile systems, WSNs, and speech and image processing.

EHAB H. ABDELHAY received the B.Sc., M.Sc., and Ph.D. degrees in communication engineering from Mansoura University, Egypt, in 2005, 2010, and 2015, respectively. He has been working as a Demonstrator at the Department of Communication and Electronics, Faculty of Engineering, Mansoura University, since 2006, a Lecturer Assistant, since 2011, and a Lecturer, since 2015. He is currently a Ph.D. Lecturer at the Faculty of Engineering, Mansoura University. His research interests include wireless telecommunication systems as 3G, 4G, and 5G mobile systems, WSNs, and speech and image processing.

HEBA Y. M. SOLIMAN (Senior Member, IEEE) received the M.Sc. and Ph.D. degrees from Suez Canal University, Egypt, in 2004 and 2010, respectively. She is currently an Associate Professor of wireless communications and signal processing with the Electrical Engineering Department, Port Said University. She is also the Executive Manager of the Entrepreneurship, Innovation and Sustainable Environment Unit, Faculty of Engineering, Port Said University. She is responsible with the Wireless Antennas Laboratory, Faculty of Engineering, Port Said University. She is a member of the Machine Learning and Signals Processing Research Center. Her contributions related to efficient use of power and frequency resources in wireless communication systems.